Electronic Supplementary Material (ESI) for Sustainable Energy & Fuels.

1. LCFN shrinkage, density and relative density

Table S1 reports the shrinkage of the LCFN pellets before and after the sintering process. The table also includes the final thickness and relative density of the pellets after polishing.

Material	Green body diameter (mm)	Diameter after sintering (mm)	Green body thickness (mm)	Thickness after sintering (mm)	Final thickness after polishing (mm)	Relative Density (%)
LCFN-1	19.16	16.07	1.00	0.85	0.75	99.3
LCFN-2	19.16	16.04	1.02	0.85	0.77	99.7
LCFN-3	19.16	16.03	1.03	0.85	0.72	99.4

Table S1: LCFN pellet dimensions before and after the sintering process, density and relative density of samples.

The density of the pellets is estimated through the Archimedes principle using deionized water as a medium. The relative density of the samples, ρ_{rel}, is estimated using the following expression:

$$\rho_{rel} = \frac{\rho_{Archimedes}}{\rho_{XRD}} \cdot 100\%$$

In the previous expression, $\rho_{Archimedes}$ is the density of the sample estimated using the Archimedes principle and ρ_{XRD} is the theoretical density of the perovskite calculated based on the lattice constants estimated through Rietveld refinement of the corresponding XRD patterns.

2. Experimental setup for LCFN permeation measurements

Figure S1 shows the button cell reactor used for the investigation of exsolution on LCFN pellets. The setup consists of two outer alumina tubes with specially machined ends to allow for a proper sealing of the membrane under investigation. The latter is achieved using one gold ring on each side; the gold rings were purchased by Lux Bond & Green. Due to sealing, the active area of the membrane, i.e. the area in contact to gas-phase species, is reduced from a diameter of $16mm$ to $12.5mm$. The inner alumina tubes are used for the introduction of the flow into each side. The temperature around the vicinity of the membrane is measured using K-type thermocouples purchased by Omega Engineering. CO_2 splitting to CO takes place at the bottom side of the reactor and will be denoted as the feed side. The top side is used for the CH_4 partial oxidation to syngas and will be denoted as fuel side. The gas-phase mixture composition is quantified using an Agilent 490 Micro Gas Chromatograph.

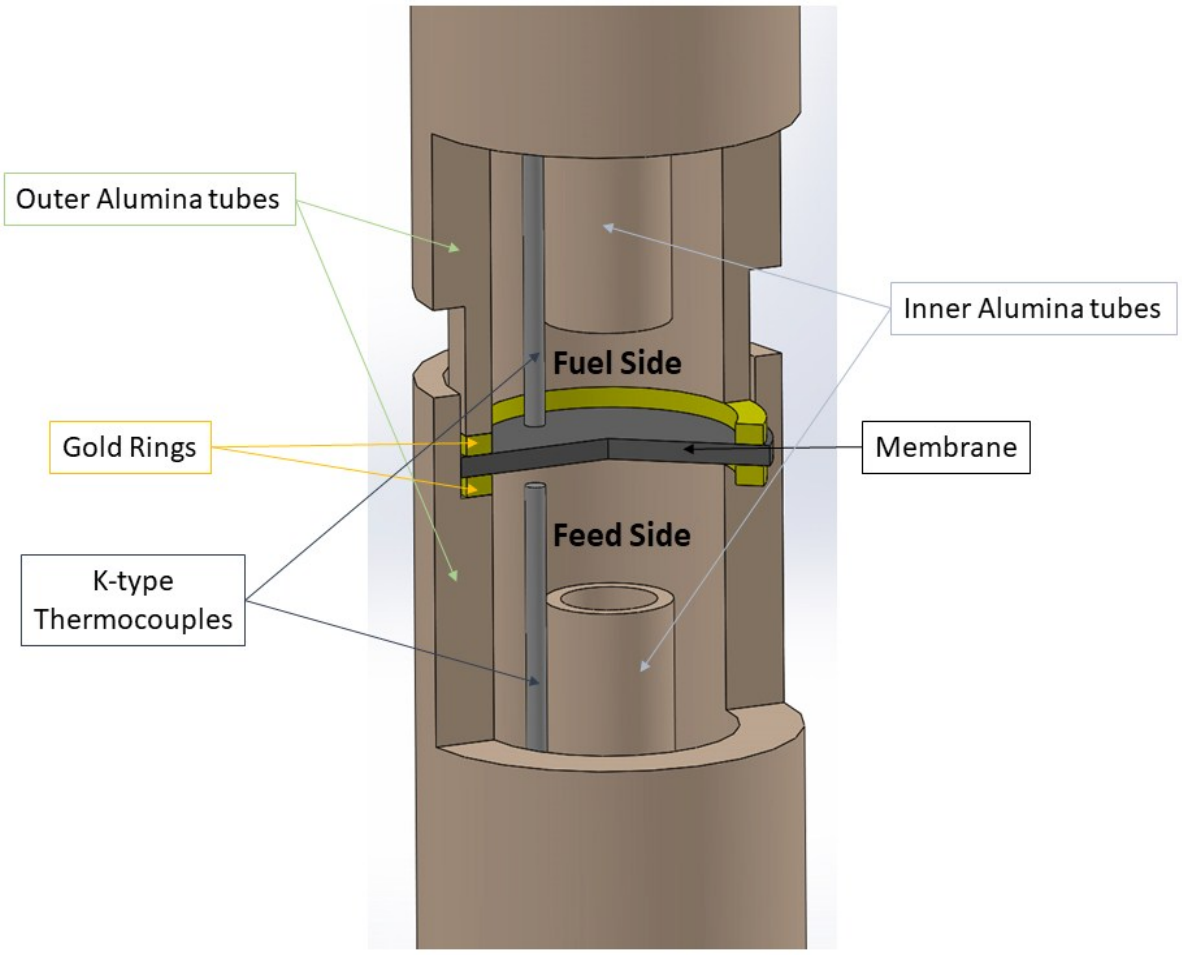

Figure S1: Button cell reactor used for the investigation of exsolution from LCFN pellets. Bottom side corresponds to the CO_2 splitting side (feed side); CH_4 partial oxidation to syngas takes place on the top side (fuel side).

3. Structural and morphological characterization of as-prepared samples

Supplementary Figure S2 shows the XRD patterns of the LCFN raw ash (prior to calcination), powder after calcination as well as the XRD pattern of the as-prepared pellets. For all three unused LCFN samples investigated in this work, the XRD patterns were identical. According to Supplementary Figure S2, the main perovskite peaks are present in the raw ash and this is due to the use of Glycine and the high temperature that evolves during the auto-ignition of the intermediate precursor mixture. As a result, the raw ash was calcined at $900℃$ for 1 hour to burn any remaining carbon and reduce particle sintering; all peaks in the calcined powders and as-prepared pellets matched well with those of $La_{0.9}Ca_{0.1}FeO_{3-\delta}$ (ICDD no. 01-082-9272).

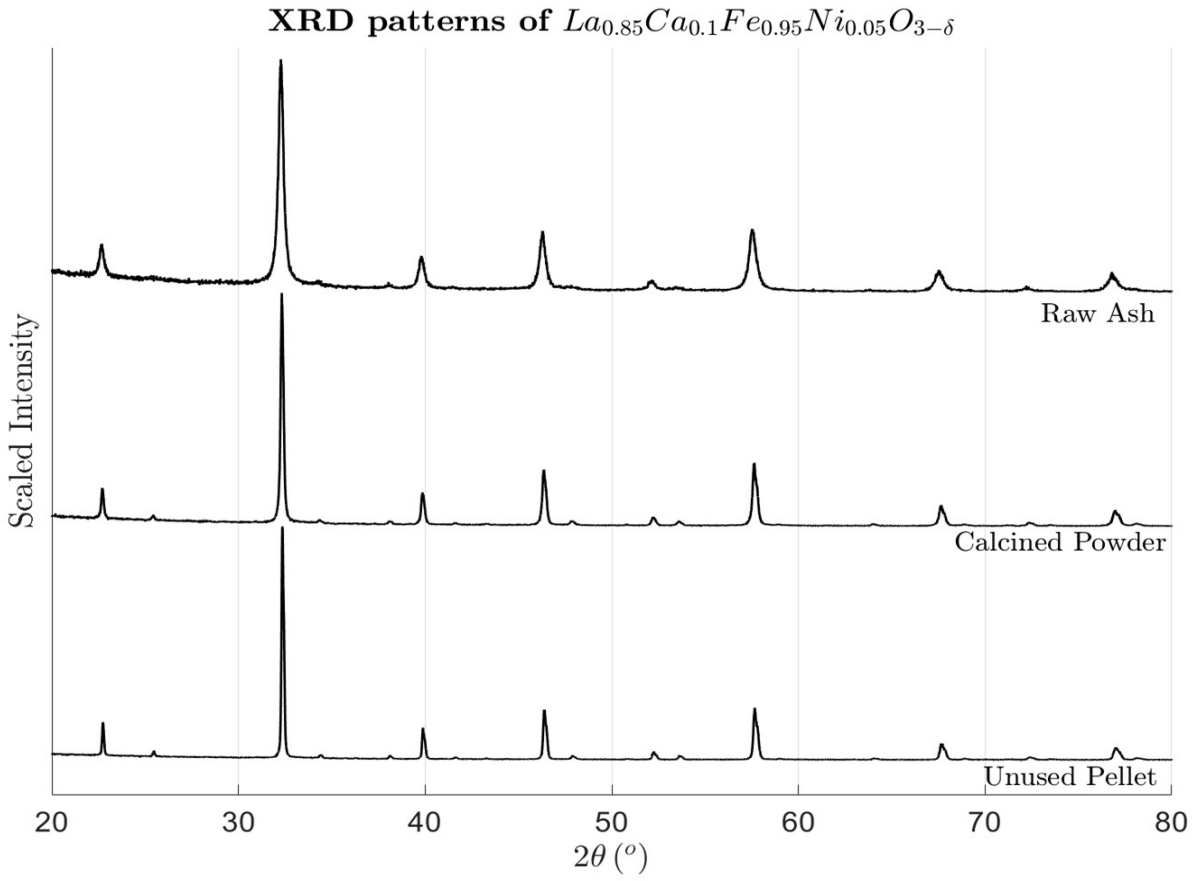

Figure S2: XRD patterns of LCFN raw ash, calcined powder and as-prepared pellet.

LCFN exhibits an orthorhombic structure ($\alpha = \beta = \gamma = 90°$) in the *Pbnm* space group. Table S2 shows the estimated lattice constants of LCFN obtained by Rietveld refinement from the XRD pattern of the LCFN pellet shown in Figure S2.

Material	Space group	Lattice constants			V_{cell} (Å^3)	V_m ($cm^3/mole$)	ρ_{XRD} (g/cm^3)
		a (Å)	b (Å)	c (Å)			
LCFN	*Pbnm*	5.535	5.539	7.823	239.84	36.11	6.260

Table S2: Space group, lattice constants, unit cell volume (V_{cell}), molar volume (V_m) and theoretical density (ρ_{XRD}) of LCFN pellet based on Rietveld refinement of the corresponding XRD pattern of an as-prepared pellet.

Figure S3 shows a SEM image of an as-prepared LCFN pellet before polishing. The grain boundaries exhibit a non-uniform size. No porosity is observed and this is consistent with the high relative density of the samples reported in this work.

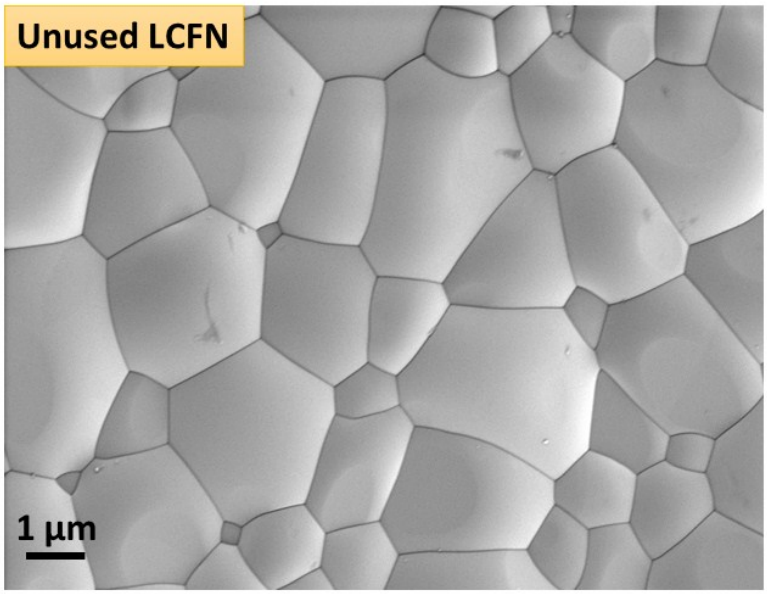

Figure S3: SEM image of the as-prepared LCFN pellet after sintering. Scale bar is in the order of 1µm.

4. EDS mapping on the fuel side of the used LCFN-3 membrane

Figure S4 shows a SEM image of the used LCFN-3 sample taken at the fuel side after the end of the permeation measurements. The EDS mapping reveals a distribution of particle sizes on the surface of the perovskite backbone as well as areas enriched in Ca, confirming the XRD results.

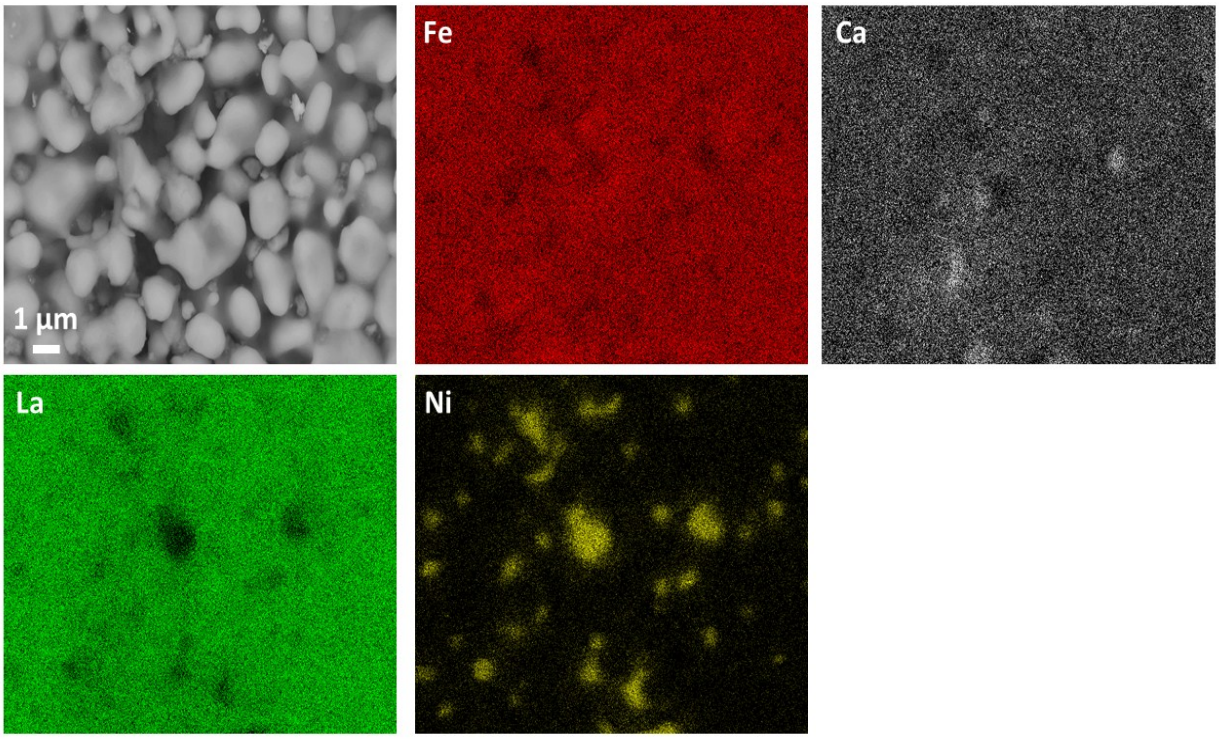

Figure S4: EDS mapping of the fuel side of the LCFN-3 pellet after the end of the measurements.

5. In situ LCFN pellet reduction in 5% H_2 inside the ceramic membrane reactor followed by permeation measurements

In this case, a LCFN pellet was introduced in the reactor shown in Figure S1. After sealing at high temperature, the temperature was set to $1000℃$ and 5% H_2 (balance Ar) was introduced on both sides of the sample to reduce LCFN prior to permeation measurements. The pellet was reduced for 15 minutes at the aforementioned conditions and then the feed side gas mixture was replaced with a mixture of $50\%\ H_2O$ (balance N_2) while 5% H_2 (balance Ar) was still flowing at the fuel side. J_{O_2} was measured and the value was $0.62 \mu mole/cm^2/sec$. The pellet was then reduced again at the same conditions for another 30 minutes and upon switching the gas to $50\%\ H_2O$ (balance N_2), J_{O_2} was reduced to $0.57 \mu mole/cm^2/sec$. A third reduction cycle for 45 minutes decreased J_{O_2} further to $0.50 \mu mole/cm^2/sec$. This shows that continuous reduction of the samples deteriorates the performance.

SEM images with a BSD confirm the presence of particles on the surface. Bright particles correspond to Ni, but these particles are large, in the order of $500nm\text{-}1\mu m$. At the same time, large chunks are found that correspond to Fe_2O_3 particles.

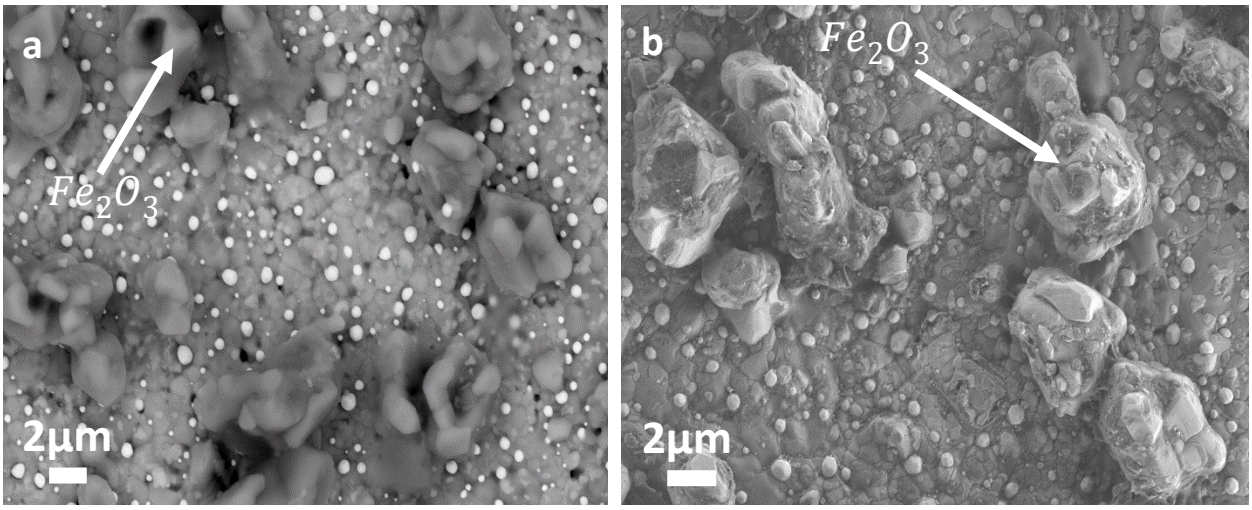

Figure S5: SEM images with BSD on the H_2O splitting side (a) and fuel side (b). Small bright particles correspond to Ni^0 while large chunks correspond to Fe_2O_3. Scale bar is at $2\mu m$.

6. XRD patterns of as-prepared and used LCFN-1 and LCFN-2 pellets

For completeness, Figures S6 and S7 show the XRD patterns of an as-prepared LCFN pellet as well as the XRD patterns on each side of the used LCFN1 ($900℃$) and LCFN-2 ($950℃$) pellets. LCFN-1 shows no additional phases on both sides, which confirms that exsolution of Ni^0 particles did not occur. The XRD patterns of LCFN-2 on both sides are identical to the LCFN-3 pellet.

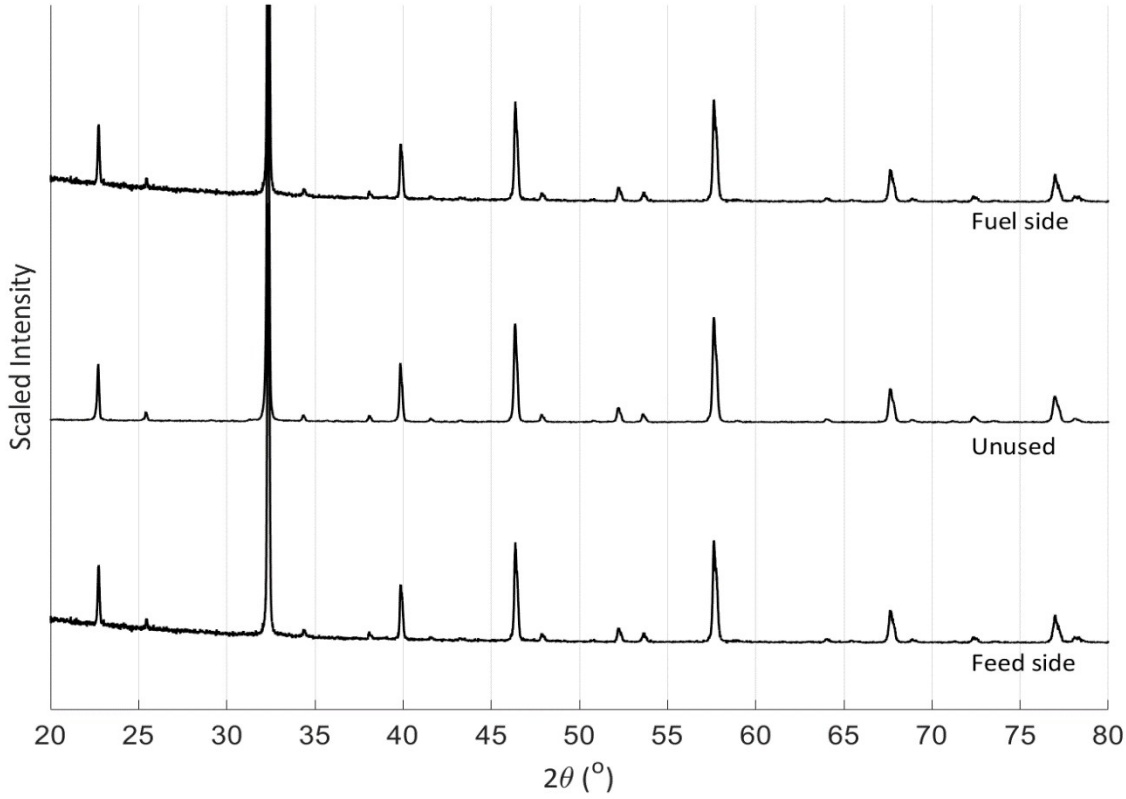

Figure S6*:* XRD patterns of an as-prepared LCFN pellet, and of the fuel and feed sides of the LCFN-1 pellet after exsolution and oxygen permeation measurements at $900℃$ as described in Figure 1 of the manuscript.

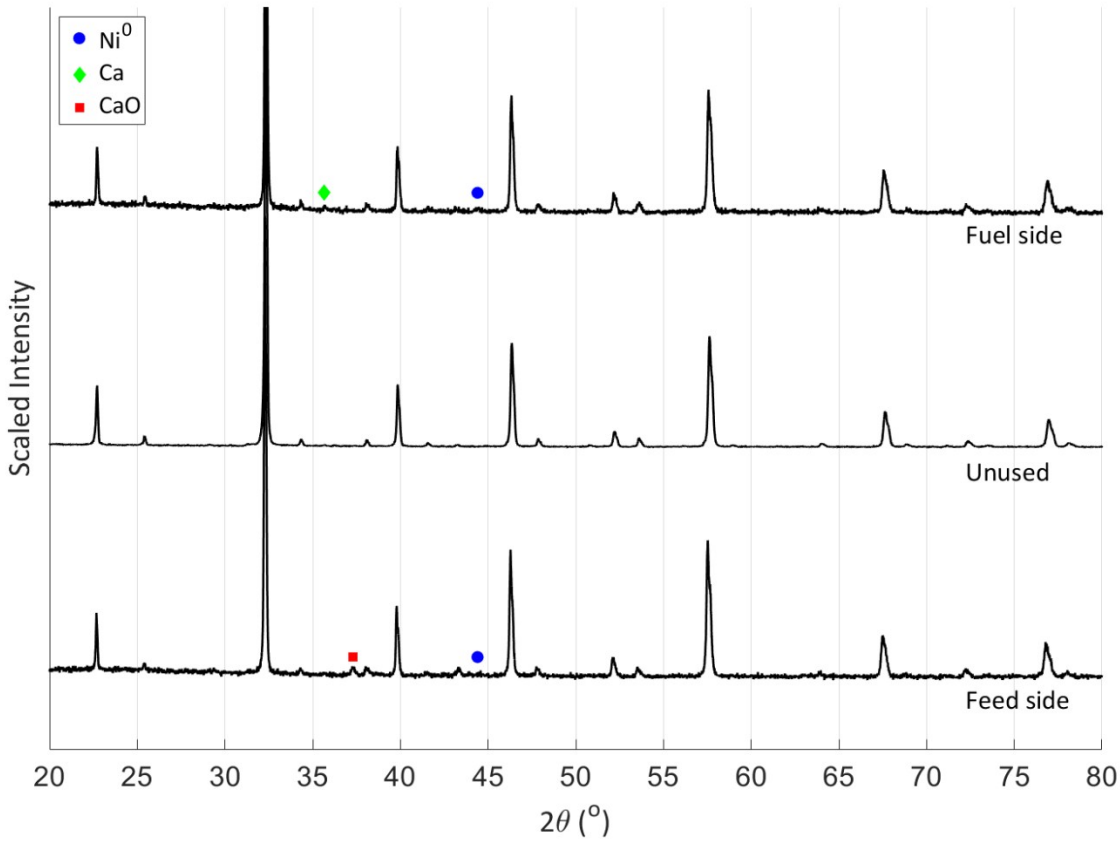

Figure S7*:* XRD patterns of an as-prepared LCFN pellet, and of the fuel and feed sides of the LCFN-2 pellet after exsolution and oxygen permeation measurements at $950^{\circ}\mathrm{C}$ as described in Figure 1 of the manuscript.